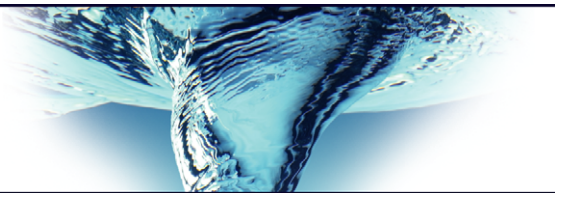
JFM RAPIDS
journals.cambridge.org/rapids



On the bubble shape in a magnetically compensated gravity environment

Jérôme Duplat[1],† **and Alain Mailfert**[2]

[1]SBT, UMR-E 9004 CEA / UJF-Grenoble 1, INAC, Grenoble, F-38054, France
[2]Labo Géoressources, Lorraine University – CNRS, ENSG Vandoeuvre-lès-Nancy, F-54500, France

(Received 24 September 2012; revised 24 September 2012; accepted 29 November 2012)

We investigate the shape of bubbles in liquid oxygen under magnetic levitation conditions: a magnetic field is applied that polarizes bulk oxygen, and its spatial variation induces a body force opposed to its weight. In these conditions, bubbles appear to have a smooth ellipsoidal shape, which may be prolate (elongated in the vertical direction), oblate (elongated in the horizontal plane) or perfectly spherical. The dependence of the elongation ratio η on the volume and levitation position is explored. It is found that the bubble shape is prescribed by the minimization of the sum of surface tension, demagnetization and magnetic–gravitational potential energies.

Key words: drops and bubbles, electrohydrodynamic effects, magnetic fluids

1. Introduction

On Earth, the shape of a static drop lying on a floor or of a static bubble lying under a ceiling depends on its size. For a small radius, the drop or bubble is perfectly spherical, while it becomes flat for larger radius. The transition radius is the capillary length $\ell_c = \sqrt{\sigma/\rho g}$ (de Gennes *et al.* 2002) for which gravitational effects equilibrate surface tension effects. Gravity affects many other physical phenomena. To understand how these processes occur in space conditions, or simply to quantify the influence of the gravity field, numerous studies have been developed to reduce or eliminate the effect of gravity. Most processes rely on the free-fall technique, but it is also possible to make use of magnetic fields to induce a body force on matter opposed to gravity. Magnetic levitation of diamagnetic bodies was already envisaged by Braunbek (1939) and the first experimental realizations in fluids were made in the 1960s (Lyon *et al.* 1965; Kirichenko & Verkin 1968). However, exact compensation cannot be obtained over a three-dimensional domain (Quettier *et al.* 2005) with a single magnetic force (Lorin & Mailfert (2009) have shown that it is possible to reach perfect compensation for diamagnetic fluids if a centrifugal force is added). For specially designed axisymmetric coils, gravity could be strictly compensated at any

† Email address for correspondence: Jerome.Duplat@ujf-grenoble.fr

 © Cambridge University Press 2013
doi:10.1017/jfm.2012.594

https://doi.org/10.1017/jfm.2012.594 Published online by Cambridge University Press

point on the axis. For standard coils, gravity is strictly compensated on two points of the axis, whose position depends on the current intensity. Stable levitation may be observed for only one of these points.

Static drops or bubbles placed in such an environment levitate around this point but are not necessarily spherical. The aim of this paper is to discuss the shape of bubbles in liquid oxygen, a paramagnetic substance. Experiments are compared to theory, which can readily be extended to any other para- or diamagnetic fluid. Previous studies discussing the shape of drops or bubbles in magnetic fields (levitating or not) have emphasized that it is determined by the competitive effect of surface tension and residual gravity force (hereafter associated with the magnetic–gravitational potential (Weilert *et al.* 1996; Nikolayev, Chatain, Beysens & Pichavant 2011; Piroird *et al.* 2012)). However, we show that a third effect plays a significant role for the case of levitating bubbles in liquid oxygen. Namely, demagnetization caused by the existence of magnetic susceptibility contrast between liquid and vapour induces an elongation of bubbles or drops in the direction of the magnetic field, as has been observed for ferro-fluid drops (Archipenko, Barkov & Bashtovoi 1979; Bacri & Salin 1982; Rosensweig 1985; Banerjee *et al.* 1999). For the case of levitating bubbles in liquid oxygen, these three effects play a significant role, and we will show that the bubble shape evolution is not monotonic with increasing bubble volume.

These three effects depend on the fact that there exists a very large density contrast between liquid oxygen and vapour, so that they are not sensitive to the exact nature of the gas. Consequently, the observation made here for oxygen gas bubbles in liquid oxygen would be unchanged for any type of gas provided the external liquid is oxygen. Our study is limited to the global shape of the bubble and does not address possible interface instabilities (Cowley & Rosensweig 1967) or the formation of conical ends (Stone, Lister & Brenner 1999). These phenomena would appear for a larger magnetic field intensity, a larger bubble size, or a larger magnetic susceptibility contrast.

2. Experimental set-up and image processing

Experiments were run in OLGA (Oxygen Low Gravity Apparatus), an experimental facility that is described in detail in Pichavant *et al.* (2009). A cylindrical cell with horizontal axis (6 cm long and 5 cm inner diameter) is placed on the vertical axis of a superconducting coil, in the outer region where the magnetic field is not uniform (see figure 1 for a schematic). Locally, the magnetic field intensity is typically 1 T and the magnetic field gradient is 4 T m^{-1}. The cell can be displaced along the vertical axis, so that several magnetic configurations can be explored. This allows one to create a magnetic body force on oxygen and compensates locally for the effect of the Earth's gravity field (see § 3). The cell is filled with liquid oxygen and oxygen vapour. For most experimental runs, the free surface stands in a region where the magnetic force is smaller than the weight, so that the free surface is stable.

The temperature of the liquid bulk is regulated with an accuracy better than 0.1 K and pressure is measured with a precision of 10 mbar. The cell is uniformly backlit. Images are captured with a 512×256 complementary metal–oxide–semiconductor (CMOS) captor, through a 3 m long endoscope and 600 mm focus lens. The visualization axis is horizontal. The outer diameter of the endoscope mirror is clearly visible on the image sequence (figure 2).

Initially, the pressure and temperature of the oxygen are set so that thermodynamic equilibrium is reached (experiments were run at $T = 80,\ 90,\ 96$ K and $P = 0.33,\ 1,\ 2$ bar, respectively). Density decreases with increasing temperature,

https://doi.org/10.1017/jfm.2012.594 Published online by Cambridge University Press

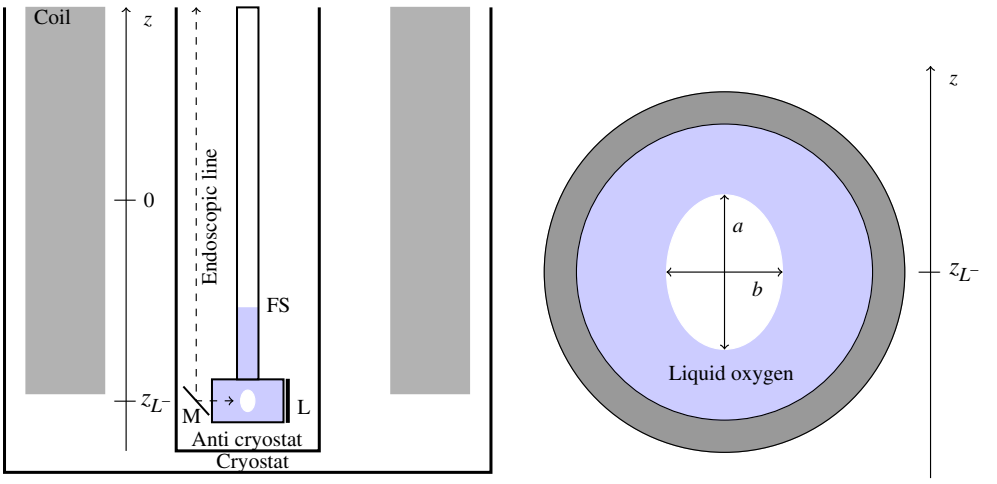


FIGURE 1. Schematic of the experimental set-up (side view) and close-up front view (i.e. camera view) of the experimental cell (FS, free surface; L, light; M, mirror). The experimental cell is filled with liquid oxygen. It is placed at the centre of a void anti-cryostat, so that it is insulated from the cryostat containing the superconducting coil ($T = 4$ K). The cryostat is approximately 3 m high. The coil is 0.55 m high. The experimental cell and the anti-cryostat can be displaced along the vertical axis together.

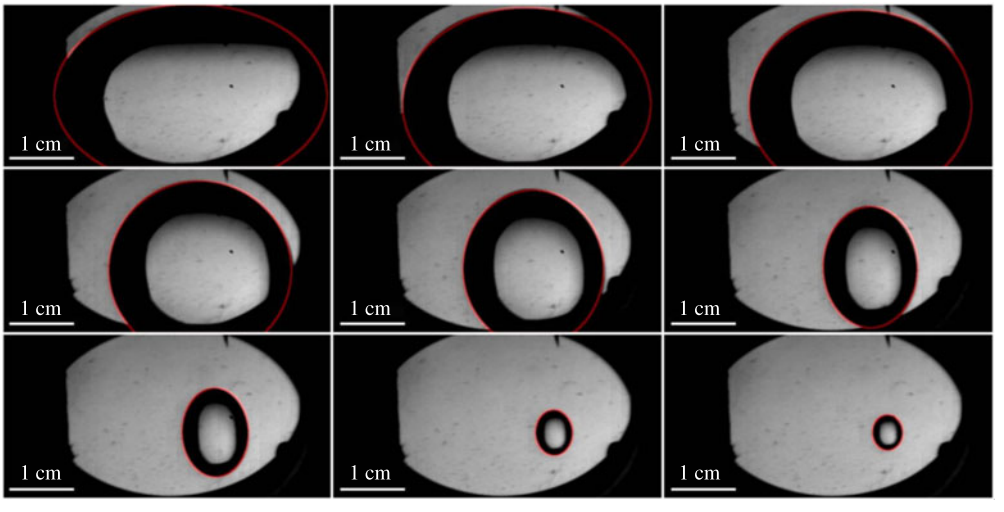


FIGURE 2. Evolution of the bubble shape as a function of its volume in liquid oxygen ($T_{bulk} = 96$ K and $i = 272$ A). The bubble shape is interpolated by an ellipse. For small volumes, the bubble is nearly spherical ($\eta \approx 1$). Increasing the volume leads to an elongation of the bubble ($\eta > 1$). For very large volumes, the bubble shape becomes flat ($\eta < 1$) and is nearly spherical at intermediate volume.

https://doi.org/10.1017/jfm.2012.594 Published online by Cambridge University Press

and so does the magnetic susceptibility χ_{mass}: the Curie–Weiss law states that

$$\chi_{mass} = \frac{1}{M}\frac{C}{(T-\Theta)}, \tag{2.1}$$

where M is the molar mass, C the Curie constant, and Θ the Curie temperature. For liquid oxygen, $C/M \approx 5.07 \times 10^{-4}$ kg K m^{-3} and $\Theta \approx -77$ K (after measurement of magnetic susceptibility at several temperatures (Lide 2005)).

A small amount of helium vapour is injected through a capillary tube into the liquid oxygen bulk. A small bubble is trapped in the levitation region that grows rapidly because of oxygen evaporation at the bubble interface. A large bubble is then obtained, composed of oxygen vapour (and a negligible amount of helium vapour). The pressure is then slightly increased, to force bubble condensation. The bubble volume decreases slowly from typically 50 to 0.1 ml in $\tau \approx 20$ s. The flow induced by bubble collapse has Reynolds number $Re = R\dot{R}/\nu \approx 100$, and the hydrodynamic pressure $\rho\dot{R}^2 \approx 10^{-3}$ Pa is small compared to the capillary pressure $2\sigma/R \approx 2$–20 Pa, so that one may consider that the experiment is quasi-static. The latent heat released during the condensation process is typically 40 J and provokes a temperature elevation in the thermal boundary layer whose thickness is $\delta_{th} = \sqrt{D\tau} \approx 2$ mm. Neglecting possible convection flow, the temperature elevation of the interface is overestimated: it is smaller than 10 K. Moreover, the initial bubble expansion is caused by evaporation, which causes a temperature damping of similar magnitude (there is no strict time reversal symmetry in the heat transfer process of the expansion–collapse cycle). This temperature fluctuation of a few kelvins has consequences for the estimation of surface tension (which may decrease by 10 % for the overestimated temperature elevation of 10 K), but does not affect the magnetic properties of the liquid bulk.

The sequence is recorded and for each frame the bubble contour is identified by thresholding the image. An ellipse with main axes in the horizontal and vertical directions is fitted to this shape by minimizing the area of the difference of the region covered by the real bubble and the fitting ellipse. The accuracy of this process is very good for small bubbles (whose entire contour is visible). It is still correct for very large bubbles, even if only a small portion of the contour is visible (see figure 2).

3. Levitation point

3.1. *Observations*

When the current intensity i in the coil is null or weak, bubbles produced in the liquid bulk rise to the surface, and no levitation is observed. For some critical value i_{min} of the current, bubbles reach an equilibrium position at some specific altitude in the coil. This corresponds to the first levitation point. For a higher current, bubbles levitate at a lower position. The absolute levitation position is not measurable with satisfactory accuracy, so that we measure only the relative levitation position. It is defined as the bubble mass centre and it is measured for several bulk temperatures. No significant dependence on the bubble volume is observed. These measurements are reported on figure 3. For each dataset, an altitude offset is adjusted so that experiments match theoretical predictions.

3.2. *Basics of magnetic–gravity compensation*

Dioxygen molecules have a small magnetic momentum. Placed in a magnetic field, they become statistically oriented in its direction, and the whole process results in an

https://doi.org/10.1017/jfm.2012.594 Published online by Cambridge University Press

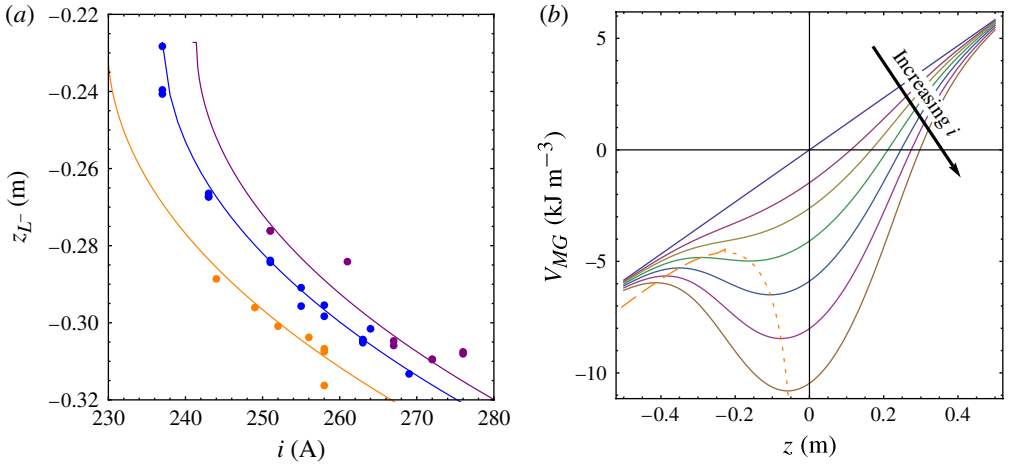


FIGURE 3. (*a*) Levitation position as a function of the current i and several temperatures (orange, $T = 80$ K; blue, $T = 90$ K; purple, $T = 96$ K). As only the relative levitation position is measurable, the altitude origin is adjusted so that each dataset matches the theoretical prediction. (*b*) Magnetic–gravitational potential profile for several current intensities, ranging from 0 to 400 A (computed for $T = 80$ K). The dashed line corresponds to the bubble stable levitation position z_{L^-} (local maximum of V_{MG}); the dotted line corresponds to the unstable levitation position z_{L^+} (local minimum of V_{MG}).

effective body force equal to

$$\frac{\mathrm{d}\boldsymbol{F}_m}{\mathrm{d}V} = \frac{\rho\chi_{mass}}{2\mu_0}\boldsymbol{\nabla}B^2, \tag{3.1}$$

where χ_{mass} denotes the massive magnetic susceptibility of oxygen, a temperature-dependent intrinsic property of oxygen molecules. This force is then proportional to the local density ρ and is conservative. One may define the magnetic–gravitational potential

$$V_{MG} = \rho\left(-\frac{\chi_{mass}}{2\mu_0}B^2 + gz\right), \tag{3.2}$$

which takes account of both magnetic and gravitational forces. Local extrema of this potential coincide at the levitation point (where magnetic forces compensate exactly the gravity force; see figure 3). For a gas bubble in suspension in a liquid, the stable levitation point coincides with the local maximum of the potential, when liquid droplets floating in gas are stable at a local minimum.

The axial induction field $B_z(0, z)$ produced by vertical axisymmetric coils in liquid oxygen is given by

$$B_z(0,z) = \frac{J\mu_0(1+\lambda\rho\chi_{mass})}{2}\left[\left(z+\frac{L}{2}\right)\log\left(\frac{R_{ext}+\sqrt{R_{ext}^2+(z+L/2)^2}}{R_{int}+\sqrt{R_{int}^2+(z+L/2)^2}}\right)\right.$$
$$\left.-\left(z-\frac{L}{2}\right)\log\left(\frac{R_{ext}+\sqrt{R_{ext}^2+(z-L/2)^2}}{R_{int}+\sqrt{R_{int}^2+(z-L/2)^2}}\right)\right], \tag{3.3}$$

https://doi.org/10.1017/jfm.2012.594 Published online by Cambridge University Press

where $J = Ni/L(R_{ext} - R_{int})$, R_{int}, R_{ext} and L denote the current density, the inner and outer diameter, and the height of the coil, respectively (the origin of the vertical axis being placed at the centre of the coil); N is the total number of turns composing the coil; and $\lambda \lesssim 1$ takes account of the exact geometry of the liquid oxygen cell. This leads to negligible corrections of the order of $\rho\chi_{mass} \approx 0.003$. In the following, it will be considered that $\lambda = 1$ for numerical applications. Owing to the axial symmetry, the eventual levitation points are located on the coil main axis. They are located at height z_L such that

$$\left.\frac{\partial V_{MG}}{\partial z}\right|_{z_L} = 0. \tag{3.4}$$

Equation (3.4) admits no solution at low intensity, and two ($z_{L^-} < z_{L^+}$) for high enough current.

The stability (with respect to a gas bubble levitating in a liquid bulk) of these solutions is obtained when $\partial^2 B^2/\partial z^2$ for the vertical stability, on the one hand, and $\partial^2 B^2/\partial r^2$ for the radial stability, on the other, are negative. The magnetic–gravitational potential curvature in the vertical and horizontal directions are given by

$$\begin{cases} \left.\dfrac{\partial^2 V_{MG}}{\partial z^2}\right|_{z_L} = -\rho\left(\dfrac{\chi_{mass}}{2\mu_0}\right)\left.\dfrac{\partial^2 B_z^2}{\partial z^2}\right|_{z_L}, \\ \left.\dfrac{\partial^2 V_{MG}}{\partial r^2}\right|_{z_L} = -\rho\left(\dfrac{\chi_{mass}}{2\mu_0}\right)\left[-\dfrac{1}{2}\left.\dfrac{\partial^2 B_z^2}{\partial z^2}\right|_{z_L} + \dfrac{3}{2}\left(\left.\dfrac{\partial B_z}{\partial z}\right|_{z_L}\right)^2\right], \end{cases} \tag{3.5}$$

as a consequence of the harmonicity and axisymmetry of B. It is then impossible to obtain a stable levitation point in both vertical and radial directions for a paramagnetic liquid droplet (as $\partial^2 V_{MG}/\partial r^2$ is necessarily negative if $\partial^2 V_{MG}/\partial z^2$ is positive). For a gas bubble the stable levitation position is z_{L^-}. Numerical solutions of (3.4) are compared with experimental observations with satisfactory agreement (figure 3).

4. Bubble shape

4.1. *Observations*

The bubble stabilizes around its equilibrium position z_{L^-} and has a smooth shape that is not necessarily spherical. On the contrary, it is observed that the bubble shape depends on the equilibrium position z_{L^-} (or equivalently on the current i) and on the bubble volume $V = (4\pi/3)R^3$, where R is the equivalent bubble radius. For small sizes ($R < 2$ mm), the bubble is nearly spherical, and for very large sizes ($R > 2$ cm) the bubble is prolate for a small levitation current i and oblate for large values of i (corresponding, respectively, to high and low levitation position). For intermediate volumes, a prolate shape is always observed, whatever the levitation current employed.

The bubble conserves axisymmetry, so that an ellipsoid shape is matched over the bubble, and the vertical a and horizontal b axes are measured. The aspect ratio of the bubble,

$$\eta = \frac{a}{b}, \tag{4.1}$$

quantifies the bubble deformation ($\eta = 1$ for pure sphere, $\eta > 1$ for prolate bubbles, and $\eta < 1$ for oblate bubbles). The dependence of η on bubble volume is reported for several currents in figure 4.

https://doi.org/10.1017/jfm.2012.594 Published online by Cambridge University Press

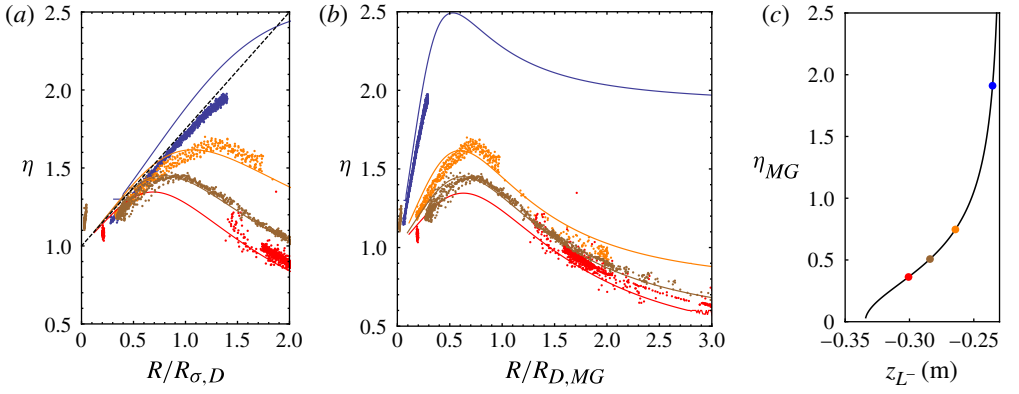


FIGURE 4. Bubble aspect ratio η as a function of the equivalent radius R. Experiments are performed with bulk temperature $T = 90$ K and current $i = 237.5,\ 243,\ 251$ A (respectively, blue, orange and brown) and with $T = 93$ K for $i = 269$ A (red). (*a*) For small bubble, $\eta \approx 1 + 3R/4R_{\sigma,D}$ (dashed line). (*b*) For large bubble, a transition occurs: for $R/R_{D,MG} < 1$, demagnetization effects dominate and the bubble is prolate; for $R/R_{D,MG} > 1$, the bubble shape is prescribed by the magnetic–gravitational isopotential surface, and $\eta \to \eta_{MG}$. (*c*) Plot of η_{MG}. Values for R_σ, D and $R_{D,MG}$ are given in table 1.

i (A)	237.5	243	251	269
$R_{\sigma,D}$ (mm)	6.5	7.5	8.2	8.2
$R_{D,MG}$ (mm)	31	13	10	9.0

TABLE 1. Characteristic transition length scales for experimental conditions of figure 4.

4.2. *Three energies*

The bubble shape is determined by the competitive effects of three energies.

4.2.1. *Surface tension*

The creation of interfacial area between liquid bulk and liquid has an energetic cost, proportional to bubble area ($V^{2/3}$). If this effect was the only one, the bubble shape would be perfectly spherical ($\eta_\sigma = 1$). The capillary energy of an ellipsoidal bubble of volume V and aspect ratio η is

$$\begin{cases} E_\sigma = \sigma 2\pi \left(\dfrac{3V}{4\pi\eta}\right)^{2/3} \left(1 + \eta^2 \dfrac{\cos^{-1}(1/\eta)}{\sqrt{\eta^2 - 1}}\right) & \text{for } \eta > 1, \\ E_\sigma = \sigma 2\pi \left(\dfrac{3V}{4\pi\eta}\right)^{2/3} \left(1 + \eta^2 \dfrac{\cosh^{-1}(1/\eta)}{\sqrt{1 - \eta^2}}\right) & \text{for } \eta < 1. \end{cases} \tag{4.2}$$

4.2.2. *Demagnetization energy*

In the presence of an external applied field $\boldsymbol{H}$ (that might be considered homogeneous), the liquid bulk without a bubble is magnetized. The magnetization field, which is uniform, is $\boldsymbol{M} = \rho\chi_{mass}\boldsymbol{H}$, giving an induction $\boldsymbol{B} = \mu_0(1 + \rho\chi_{mass})\boldsymbol{H}$. When there is a vapour bubble, its internal magnetization is lower than this of the

https://doi.org/10.1017/jfm.2012.594 Published online by Cambridge University Press

liquid bulk. So, the induction field is modified inside and outside the bubble, giving rise to an energy called the demagnetization energy E_D. However, for an ellipsoidal bubble, the internal field is also uniform. The internal field $\boldsymbol{H}_b$ and the demagnetizing energy have simple expressions (Fournet 1979). For axisymmetric ellipsoidal bubbles whose axis is directed along $\boldsymbol{H}$, one obtains

$$\boldsymbol{H}_b = \frac{1+\rho\chi_{mass}}{1+[\rho(1-D(\eta))+\rho_v D(\eta)]\chi_{mass}}\boldsymbol{H} \tag{4.3}$$

and

$$E_D = \frac{B(z_{L^-})^2\, V}{2\mu_0}\frac{(\rho-\rho_v)\chi_{mass}}{1+\rho\chi_{mass}}\frac{1}{1+[\rho(1-D(\eta))+\rho_v D(\eta)]\chi_{mass}}, \tag{4.4}$$

where $D(\eta)$ is the demagnetization coefficient, a decreasing function of η (from $D(0)=1$ to $D(\infty)=0$; Osborn 1945), $B(z_{L^-})$ is the induction that would result if there was no bubble, and $\rho_v \ll \rho$ is the density of the vapour. The dominant term in E_D scales like $(\rho-\rho_v)\chi_{mass}VB^2/2\mu_0$. It is related to the lowering of magnetic susceptibility inside the bubble, but it is independent of bubble shape. The interaction of the perturbation of $\boldsymbol{B}$ and liquid oxygen acts on the bubble shape. It scales like $D(\eta)\,(\rho-\rho_v)^2\,\chi_{mass}^2 B^2/2\mu_0$. The contribution of demagnetization to the total system energy is proportional to the bubble volume. It tends to make the bubble very elongated ($\eta=\infty$, that is, $D_\infty=0$). Here we have assumed that $\boldsymbol{H}$ is homogeneous on length scales comparable with the bubble size (the relative intensity of the magnetic field second harmonic is small, $a\partial_z H/H|_{z_{L^-}} < 0.05$, so that the relative energy underestimation is of the order of 25×10^{-4}).

4.2.3. *Magnetic–gravitational energy*

The combined effects of gravity and magnetic field act on the oxygen molecules as a conservative force described by the magnetic–gravitational potential V_{MG}. If this force was the only one acting, the bubble shape would be fixed by the iso-V_{MG} surface. Approximating the magnetic–gravitational potential by a quadratic expression, the latter is an ellipsoid of aspect ratio $\eta_{MG}=[(\partial^2 V_{MG}/\partial r^2)/(\partial^2 V_{MG}/\partial z^2)]^{1/2}$ (see figure 4).

For an arbitrary bubble shape η and volume V, one may define the magnetic–gravitational energy of the bubble, associated with the absence of liquid in the bubble volume, as

$$E_{MG} = VV_{MG}(z_{L^-}) - V^{5/3}\left(\frac{3}{4\pi\eta}\right)^{2/3}\left[\frac{\eta^2}{5}\left.\frac{\partial^2 V_{MG}}{\partial z^2}\right|_{z_{L^-}} + \frac{2}{5}\left.\frac{\partial^2 V_{MG}}{\partial r^2}\right|_{z_{L^-}}\right]. \tag{4.5}$$

The shape-dependent part of bubble magnetic–gravitational energy is proportional to $V^{5/3}$, which makes this term dominant for a very large bubble. Note that the demagnetization field (discussed above) is proportional to the magnetic susceptibility ($\rho\chi_{mass}$) so that it has negligible effect on the magnetic–gravitational potential.

4.3. *Bubble shape*

The bubble shape minimizes the total energy of the system,

$$E(\eta, V) = E_\sigma + E_D + E_{MG}. \tag{4.6}$$

https://doi.org/10.1017/jfm.2012.594 Published online by Cambridge University Press

This function is numerically minimized (with respect to η) and compared to experimental results (figure 4). Physical properties are estimated for the liquid bulk temperature (so that the surface tension is slightly underestimated, as discussed above). No fitting parameters are used, and the agreement between theoretical predictions and experimental observations is very good. We attribute the observed small discrepancies to uncertainties in the geometrical properties of the coil. It is observed that the sensitivity of the aspect ratio curve to levitation position is strong. The latter depends on the liquid magnetic susceptibility, and on the coil structure (number of turns). These quantities are known with an accuracy of the order of 1 %, which induces a typical error of 0.1 for the aspect ratio prediction. For the $i = 269$ A experimental run, the free surface separating liquid and vapour was in an inverted gravity zone, so that vapour bubbles were regularly entrained towards the liquid bulk, because of Rayleigh–Taylor instability. The bubbles condense, causing latent heat release and temperature elevation in the liquid bulk. The free surface is transitorily cooled, in order to force vapour bubbles to condense near the interface. The entrainment process is then stopped during the measurement of bubble aspect ratio, so that it is not affected by any spurious flow. However, temperature inhomogeneities are not cancelled. For this run, the liquid bulk temperature is close to 93 K, but significant fluctuations (of the order of 1–2 K) might be observed.

4.4. *Characteristic length scales*

The bubble shape is determined by the competitive effects of three energies. The dominant effect depends on the bubble radius, and one may compare capillary and demagnetization intensity, and define

$$R_{\sigma,D} = \frac{6\sigma\mu_0}{B^2\,(\rho\chi_{mass})^2}. \tag{4.7}$$

For $R = (3V/4\pi)^{1/3} < R_{\sigma,D}$, capillary effects are dominant, and the bubble is nearly spherical (see figure 4). Expanding (4.6) for $R \ll R_{\sigma,D}$ and $\eta \approx 1$, one gets

$$\eta \approx 1 + \frac{3}{4}\frac{R}{R_{\sigma,D}}. \tag{4.8}$$

Demagnetization and magnetic–gravitational effects should also be compared. One defines

$$R_{D,MG} = \sqrt{\frac{\rho\chi_{mass}B^2}{\partial^2 B^2/\partial z^2}}. \tag{4.9}$$

For $R_{D,\sigma} < R < R_{D,MG}$, the demagnetization effects are stronger and the bubble is prolate. Finally, for $R > R_{D,MG}$, the bubble shape is fixed by the iso-magnetic–gravitational potential surface. The transition is clearly visible on figure 4.

5. Conclusions and further remarks

The magnetic levitation of bubbles in liquid oxygen is possible by applying a strong magnetic field gradient. Vapour bubbles (whatever their composition) reach an equilibrium position that is stable in both vertical and horizontal directions. The bubble shape is determined by the competitive effects of three energies, whose relative intensities depend on the bubble size, compared with $R_{\sigma,D}$ and $R_{D,MG}$.

https://doi.org/10.1017/jfm.2012.594 Published online by Cambridge University Press

5.1. *Levitation of diamagnetic droplets*

As has been discussed, it is also possible to levitate diamagnetic drops (like hydrogen or water). In this case, the drop shape is also given by the competitive effects of capillarity, demagnetization and magnetic–gravitational potential. However, diamagnetic fluids have a very weak magnetic susceptibility ($-\rho\chi_{mass} < 10^{-6}$). Consequently, very strong magnetic energy gradients have to be applied (approximately 1000 $\mathrm{T}^2\ \mathrm{m}^{-1}$ for hydrogen). However, the demagnetization effects become vanishingly small, as they are proportional to $(\rho\chi_{mass})^2$. The drop shape is then given by only the interaction of magnetic–gravitational potential and surface tension, as observed by Weilert *et al.* (1996). The characteristic transition radius is

$$R_{\sigma,MG} = \left(\frac{6\sigma\mu_0}{\rho\chi_{mass}\partial^2 B^2/\partial z^2}\right)^{1/3} = R_{\sigma,D}^{1/3} R_{D,MG}^{2/3}. \tag{5.1}$$

Working near the critical condition, capillary effects vanish as well, and the iso-magnetic–gravitational potential surface are made visible (Lorin *et al.* 2009).

5.2. *Effects of magnetic field in gravity free environment*

The bubble or drop shape of a magnetic material in a gravity-free environment is also affected by the existence of a magnetic field. In this case, the levitation is a direct consequence of the absence of gravity, and we can consider the effect of a uniform magnetic field of intensity B. The magnetic–gravitational potential is uniform, and the bubble shape is determined by only the surface tension and the demagnetization effect. The transition radius between a pure sphere and an elongated cylinder is $R_{\sigma,D}$, as observed for ferro-fluid droplets in confined geometry (Flament *et al.* 1996; Banerjee *et al.* 1999).

5.3. *Final remark*

The use of magnetic levitation for the study of the consequence of the absence of gravity is convenient but not absolutely perfect. Major efforts have been made to reduce the inhomogeneities of the magnetic force. If the quest for perfect gravity compensation is in vain, the use of a larger coil and subtle magnetic configuration allows that the residual effective gravity be small over larger volumes (for oxygen, we have a relative gravity smaller than 1.5 % in a volume of 4 cm^3). We would like to emphasize the role of demagnetization. This second-order term (it is proportional to $(\rho\chi_{mass})^2$) is shown to be crucial in our experimental conditions. Its relative importance would be even larger if better homogeneity of magnetic compensation could be obtained. In order to reduce the effect of demagnetization, it is worth working at a lower magnetic field intensity B. However, the levitation condition prescribes the value of $B\partial B/\partial z$. In this paper we have only discussed the demagnetization effect of a constant magnetic field. However, the demagnetization effect in a uniform magnetic field gradient is very similar: the intensity of the demagnetization energy is proportional to B^2 for a uniform field and to $(a\partial B/\partial z)^2$ in a uniform gradient. The effects of demagnetization are minimized if these two terms have similar magnitude. However, in the usual magnetic configurations for levitation, this condition corresponds to a very weak homogeneity of the residual gravity. The understanding and quantification of all these spurious effects of magnetic–gravity compensation are essential for a correct interpretation of the experimental observations.

https://doi.org/10.1017/jfm.2012.594 Published online by Cambridge University Press

Acknowledgement

We thank J. Chartier and D. Chatain for technical support.

References

ARCHIPENKO, V. I., BARKOV, YU. D. & BASHTOVOI, V. G. 1979 Shape of a drop of magnetized fluid in homogeneous magnetic field. *Magnetohydrodynamics* **14** (3), 373–375.

BACRI, J. C. & SALIN, D. 1982 Instability of ferrofluid magnetic drops under magnetic field. *J. Phys. Lett.* **43**, L649–L654.

BANERJEE, S., FASNACHT, M., GAROFF, S. & WIDOM, M. 1999 Elongation of confined ferrofluid droplets under applied fields. *Phys. Rev.* E **60**, 4272–4279.

BRAUNBEK, W. 1939 Freies Schweben diamagnetischer Körper im Magnetfeld. *Z. Phys.* A*: Hadrons Nuclei* **112** (11), 764–769.

COWLEY, M. D. & ROSENSWEIG, R. E. 1967 The interfacial stability of a ferromagnetic fluid. *J. Fluid Mech.* **30** (4), 671–688.

FLAMENT, C., LACIS, S., BACRI, J.-C., CEBERS, A., NEVEU, S. & PERZYNSKI, R. 1996 Measurements of ferrofluids surface tension in confined geometry. *Phys. Rev.* E **53**, 4801–4806.

FOURNET, G. 1979 *Électromagnétisme*. Masson.

DE GENNES, P. G., BROCHARD-WYART, F., QUÉRÉ, D., FERMIGIER, M. & CLANET, C. 2002 *Gouttes, Bulles, Perles et Ondes*. Belin.

KIRICHENKO, Y. A. & VERKIN, B. I. 1968 Simulation of zero and reduced gravity fields for heat transfer investigations under boiling. *Dopov. Akad. Nauk Ukr. SSR, Ser. A* **7**, 637–640.

LIDE, D. R. (Ed.) 2005 *Handbook of Chemistry and Physics*, 86th edn. CRC, Taylor & Francis.

LORIN, C. & MAILFERT, A. 2009 Magnetic compensation of gravity and centrifugal forces. *Microgravity Sci. Technol.* **21** (1–2), 123–127.

LORIN, C., MAILFERT, A., CHATAIN, D., FÉLICE, H. & BEYSENS, D. 2009 Magnetogravitational potential revealed near a liquid-vapour critical point. *J. Appl. Phys.* **106** (3)033905.

LYON, D. N., JONES, M. C., RITTER, G. L., CHILADAKIS, C. I. & KOSKY, P. G. 1965 Peak nucleate boiling fluxes for liquid oxygen on a flat horizontal platinum surface at buoyancies corresponding to accelerations between -0.03 and $1\,g_E$. *AIChE J.* **11** (5), 773–780.

NIKOLAYEV, V. S., CHATAIN, D., BEYSENS, D. & PICHAVANT, G. 2011 Magnetic gravity compensation. *Microgravity Sci. Technol.* **23** (2), 113–122.

OSBORN, J. A. 1945 Demagnetizing factors of the general ellipsoid. *Phys. Rev.* **67** (11–12), 351–357.

PICHAVANT, G., CARITEAU, B., CHATAIN, D., NIKOLAYEV, V. & BEYSENS, D. 2009 Magnetic compensation of gravity: experiments with oxygen. *Microgravity Sci. Technol.* **21** (1), 129–133.

PIROIRD, K., DARBOIS TEXIER, B., CLANET, C. & QUÉRÉ, D. 2012 Shaping and capturing leidenfrost drops with a magnetic field. *Phys. Fluids*, arXiv:1210.5718v1.

QUETTIER, L., FÉLICE, H., MAILFERT, A., CHATAIN, D. & BEYSENS, D. 2005 Magnetic compensation of gravity forces in liquid/gas mixtures: surpassing intrinsic limitations of a superconducting magnet by using ferromagnetic inserts. *Eur. Phys. J. Appl. Phys.* **32**, 167–175.

ROSENSWEIG, R. E. 1985 *Ferrohydrodynamics*. Dover.

STONE, H. A., LISTER, J. R. & BRENNER, M. P. 1999 Drops with conical ends in electric and magnetic fields. *Proc. R. Soc. Lond.* A **455** (1981), 329–347.

WEILERT, M. A., WHITAKER, D. L., MARIS, H. J. & SEIDEL, G. M. 1996 Magnetic levitation and noncoalescence of liquid helium. *Phys. Rev. Lett.* **77** (23), 4840–4843.

https://doi.org/10.1017/jfm.2012.594 Published online by Cambridge University Press